Lasers in Manufacturing Conference 2021

Comparison of ultrafast laser ablation of CrMnFeCoNi high antropy alloy to the conventional stainless steel AISI 304

D. Redka[a,c], C. Gadelmeier[b], J. Winter[a], M. Spellauge[a], J. Minár[c], H. P. Huber[a,*]

[a]*Department of Applied Sciences and Mechatronics, Hochschule München University of Applied Sciences, Germany*
[b]*Metals and Alloys, University of Bayreuth, Germany*
[c]*New Technologies-Research Center, University of West Bohemia, Czech Republic*

Abstract

Ultrafast lasers as tools are nowadays mainly used in the field of high-precision laser micromachining. However, for technical applications, besides process optimization, the development of new functional materials is of crucial importance. In this work, we present a novel study on single-pulse laser ablation (530 fs, 1056 nm) of CrMnFeCoNi high entropy alloy (HEA), and compare results to the conventional stainless steel AISI 304. While HEAs are known to have a high damage resistance against high-energy particle radiation we find that this is not true for electromagnetic radiation, as the damage threshold of CrMnFeCoNi HEA is 0.24 J/cm², which is lower than that of AISI 304 (0.27 J/cm²). A detailed analysis of the crater morphology, ablation depths as well as ablation volumes shows that the ablation mechanisms for both alloys are comparable, but contrary to expectations, CrMnFeCoNi HEA laser ablation is energetically more efficient in comparison to AISI 304.

Keywords: High entropy alloy; Stainless steel; Ultrashort-pulse; Threshold fluence; Ablation energetic;

1. Introduction

High entropy alloys (HEA) are a novel group of materials and are defined, among others, by consisting of at least 5 alloying elements in approximately the same atomic concentration [1]. Hereby, the binding enthalpy is significantly minimized from the maximized configuration entropy, leading to a stable formation of a solid-solution phase. This approach differs from conventional alloy design, where properties of a metal are optimized by admixture of small amounts of alloying elements (minor elements). However, by appropriate selection of principle elements (concentration < 5%), mechanical, magnetic or thermodynamic properties of

* Corresponding author. Tel.: +49-89-1265-1686; fax: +49-89-1265-1603
E-mail address: heinz.huber@hm.edu

HEAs can be tailored from scratch. This approach opened a new focus in material research with the discovery of a stable concentrated solid solution phase with nearly equiatomic concentration, namely the CrMnFeCoNi alloy by Cantor et al. in 2004 [2]. Since then, numerous high entropy alloys have been developed as well as their physical properties investigated. It appears that HEAs are in general a promising candidate for a wide group of advanced functional materials for technical applications. These include applications for environmental protection, energy storage as electrochemical supercapacitor, electromagnetic wave absorption materials for communication industry, thermoelectric materials or even as superconducting materials [3]. HEAs were also shown to have excellent mechanical properties such as high strength-to-weight ratio, high yield strength, fracture toughness and corrosive resistivity, which makes them suitable for structural materials and technical applications such as aerospace engineering [4]. In addition to these attributes, damage tolerance to high-energy particle radiation is of high importance for aerospace engineering structural materials and nuclear applications [5]. The improved radiation tolerance of HEAs is attributed to the increased chemical complexity and the resulting reduced point defect diffusion. It follows that for heavy ion bombardment of CrMnFeCoNi, irradiation-induced voids are much smaller compared to Ni or binary solid solutions such as NiCo, since 3D migration of induced defect sites and recombination with interstitial atoms strongly attenuate void nucleation [6]. Experiments with He ions irradiation also showed that CrMnFeCoNi itself exhibits reduced size of induced nano voids in the material compared to AISI 304 stainless steel (Fe72Cr18Co10), resulting in lower radiation induced material swelling. Increased stacking fault density in CrMnFeCoNi compared to AISI304, due to lower point defect diffusion, also instigates greater hardening after particle radiation [7].

So far, there are hardly any investigations on laser-matter interaction in the field of micro-material processing of high entropy alloys. In general, ultrashort pulse (USP) laser systems offer severe advantages over longer nanosecond pulses. Especially the increased precision of micro material processing [8] and higher ablation efficiency of femtosecond pulses compared to picosecond pulses [9] is of high interest. However, process understanding, and its optimization is of great importance to the industry for future technical application. Therefore, in this proceeding, we present our results on sub ps laser ablation of the high entropy alloy CrMnFeCoNi alloy and compare them with the conventional stainless steel AISI 304 in order to investigate possible peculiarities due to the increased configuration entropy. We chose AISI 304 as prospect candidate based on the equal fcc crystal lattice structure, chemical composition and comparable physical properties. In order to exclude material dependent heat accumulation and incubation effects, which play a major role in multipuls material processing [10], single pulse experiments were performed. We present results on ablation threshold, crater morphology and topology as well as an energetic consideration.

2. Materials and Methods

The polycrystalline equiatomic CrMnFeCoNi alloy (deviation less than 1 at. %) was prepared by arc melting and directed solidified in the [001] orientation (see ref. [11,12]). The average grain size is 150 – 180 µm. The CrMnFeCoNi as well as the AISI 304 samples were plane ground and polished in several successive polishing steps (9, 3, 1 µm polycrystalline diamond suspension) to a surface roughness below 2 nm. The optical penetration depth of both substrates was determined using ellipsometry measurements (Sentech SE 850) according to $\delta_{opt} = \lambda/(4\pi\kappa)$. Likewise, the reflectance.

Single-pulse ablation experiments were performed using an Nd:Glass femtosecond laser source with a central wavelength of 1056 nm (spectral width $FWHM$ = 5 nm), a pulse duration of 530 fs, and a beam quality of M^2<1.4. The maximum pulse energy of the laser is 60 µJ and individual pulses, emitted at a repetition rate of 500 Hz, were selected with a mechanical shutter. The laser beam was focused on the sample using an f = 100 mm plano-convex lens, with a beam waist radius of approximately 15 µm an a Rayleigh length of 0.5 mm.

Thus, single pulse laser ablation experiments with fluences ranging from 0.1 J/cm² to 10 J/cm² were performed on both alloys.

To determine the ablation threshold (D^2 Method), the crater diameters were measured with a light microscope (Leitz Ergoplan (50x/0.85)). The surface topography was recorded by interferometric confocal microscopy (Sensofar Plμ 2300, 50x/0.42 objective, interferometric mode) and the crater depths, profiles and volumes were determined from these data sets.

3. Results and Discussion

3.1. Ablation Threshold

The ablation threshold fluence was determined using the D²-Method [13] and is given by

$$D^2 = 2\, w_0 \ln\left(E_p / E_{thr}\right), \tag{1}$$

where w_0 is the beam waist radius, D^2 the measured squared crater diameter and E_p and E_{thr} the corresponding pulse energy and energy threshold, respectively. The ablation threshold fluence (peak fluence) is calculated for the Gaussian beam via $\Phi_{thr} = 2\, E_{thr}/\pi\, w_0^2$. The measurement data and model fit are given in Figure 1a. The deviation of the excluded data, starting from a fluence of about 3 – 4 J/cm², is attributed to the beam quality, resulting in a contribution of small satellites (deviation from the TEM_{00} mode) to the ablation process [14]. The model fit yields in an ablation threshold of 0.24(1) J/cm² and 0.27(1) J/cm² for the CrMnFeCoNi alloy and AISI 304, respectively. Literature values with comparable laser parameter show for AISI 304 an ablation threshold between 0.2 J/cm² and 0.3 J/cm² [15–17]. We thus find that CrMnFeCoNi alloy has a slightly lower ablation threshold than AISI 304, which may not be explained by considering the material specific reflectance. Here, we determined an absorbance of CrMnFeCoNi as well as AISI 304 of 29.3(1) % and 31.6(1) %, respectively, resulting in an absorption-corrected ablation threshold of 70(3) mJ/cm² and 85(3) mJ/cm².

3.2. Crater Morphology and Topography

The crater morphology of the two investigated alloys is shown for two fluences (0.4 J/cm² and 2.1 J/cm²) in the SEM images of Figure 1c (left AISI 304, right CrMnFeCoNi alloy). On first observation, nano-groves on the CrMnFeCoNi alloy surface are noticeable. These are caused by local field enhancement on surface nano-scratches on the pristine surface [18], which are a leftover from the polishing process. Due the negligible volume ratio, an influence on the global ablation process as well as the energetics is excluded [11]. Further, it can be seen in the SEM images that for AISI 304, close to the ablation threshold (0.4 J/cm²), a closed rim has been established at the crater boundary. This phenomenon is not seen for the CrMnFeCoNi alloy presumably due to the interruptions caused by the nano-groves. Furthermore, at the low fluence, both craters qualitatively show a low surface roughness. This roughness remains for AISI 304 in the 2.1 J/cm² ablation craters, where the CrMnFeCoNi alloy already shows in the center of the ablation crater an onset of re-solidified molten material. This transition is well seen in the ablation depth data (see Figure 1b) for fluences above 3 J/cm² and is attributed to the onset of melt expulsion, which occurs during / after phase explosion [19]. From the evaluation of the ablation depths, it appears that for both alloys when processed with 530 fs pulses, the Beer-Lambert law described the energy deposition sufficient with $\delta_{abl} = \delta_{eff} \ln(\Phi_0/\Phi_{thr})$, where δ_{eff} is the effective penetration depth (see fit in Figure 1b). The determination of the effective penetration depths as 15.0(3) nm and 16.3(9) nm

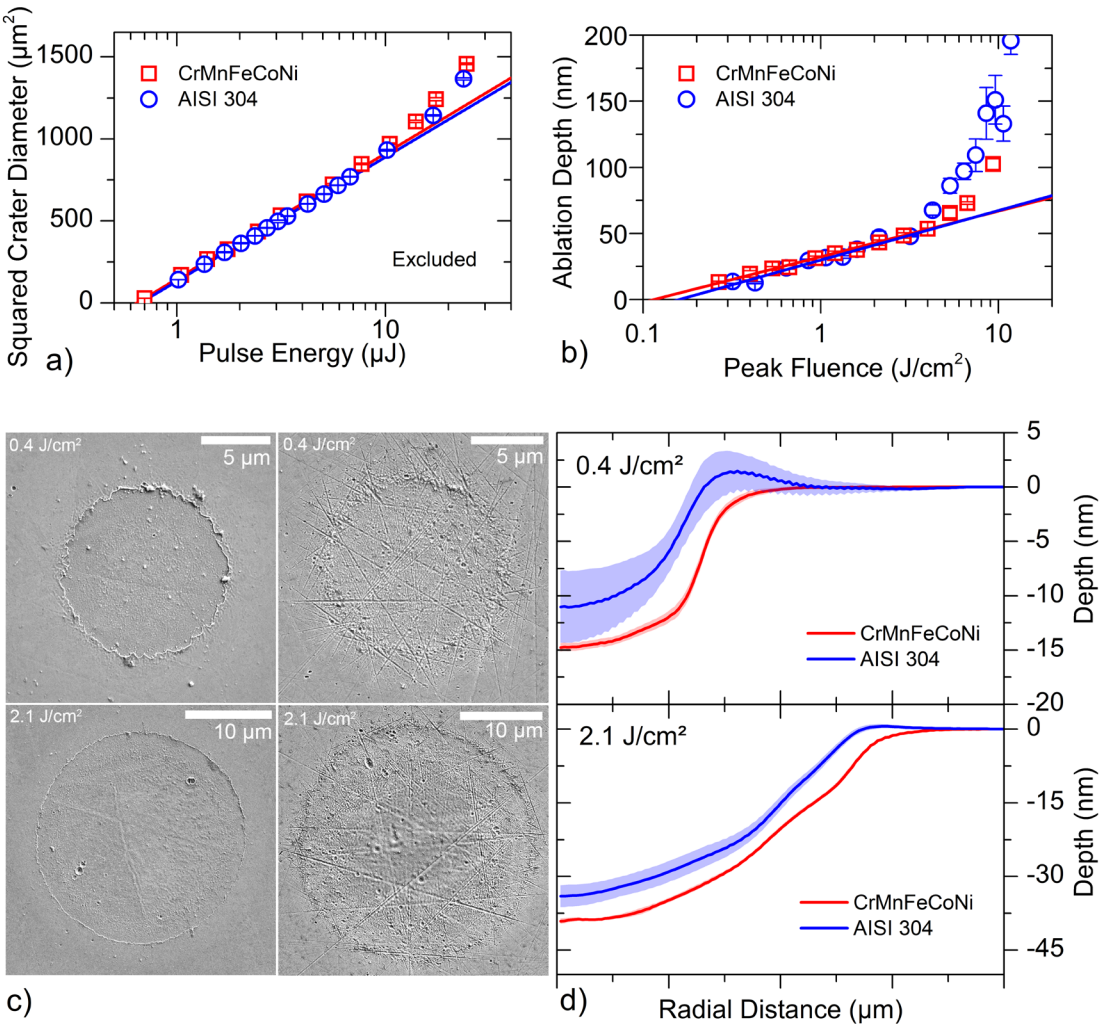

Fig. 1. (a) D^2 method for ablation threshold determination; (b) fluence dependent ablation depths; (c) SEM images for CrMnFeCoNi (left column) and AISI 304 (right column) for 0.4 J/cm² and 2.1 J/cm²; (d) corresponding radial crater profiles

for CrMnFeCoNi alloy and AISI 304, respectively, shows that they are in good agreement with the optical penetration depth of 15.6(1) nm and 17.0(1) nm. This is explained by the high electron-phonon coupling as well as low thermal conductivity of both alloys [20,21] and thus the effective penetration depth ($\delta_{eff} = \delta_{opt} + \delta_{diff}$) is dominated by the optical penetration depth. The radial mean crater cross sections, evaluated from the crater topology, are given for the fluences analogous from the SEM images in Figure 1d. For 0.4 J/cm², slightly above the ablation thresholds, the CrMnFeCoNi alloy exhibits a more rectangular profile. For AISI 304, the crater rim (see SEM images in 1c) can be seen as a pronounced elevation. For the high fluence of 2.1 J/cm² both crater profiles show a comparable trend (parabolic nature in first approximation). The depth of the CrMnFeCoNi crater is slightly higher, which is referred to the lower ablation threshold. In summary, the crater morphology and topography differ only slightly for both alloys.

3.3. Ablation Efficiency and Energetic Consideration

The energy-specific ablation volume (ESAV) is the ablation volume divided by the pulse energy and serves as a measure of the efficiency of the ablation process. Figure 2 shows the ESAV curves calculated from the measured ablation volumes for the two investigated alloys. Here, the pulse energies were corrected with the measured absorption of the materials, which are at 1056 nm wavelength 29.3(1) % and 31.6(1) % for CrMnFeCoNi alloy and AISI 304, respectively. The variation of the ESAV for both alloys is in good agreement with the ablation model according to Furmanski et al. [22] (see solid lines in Figure 2) which is described within

$$\mathrm{ESAV}=(\delta_{\mathrm{eff}}/A)\left(\ln^2(\Phi_0/\Phi_{\mathrm{thr}})/2\,\Phi_0\right). \tag{2}$$

The measured ESAV maxima are located at about 4.5-times the ablation threshold for both alloys and the absorption corrected ESAV values are 9.8(8) µm³/µJ and 6.7(5) µm³/µJ (equivalent to 101(8) J/mm³ and 149(11) J/mm³) for the CrMnFeCoNi alloy and AISI 304, respectively. Thus, the high entropy alloy shows higher ablation efficiency than the stainless steel.

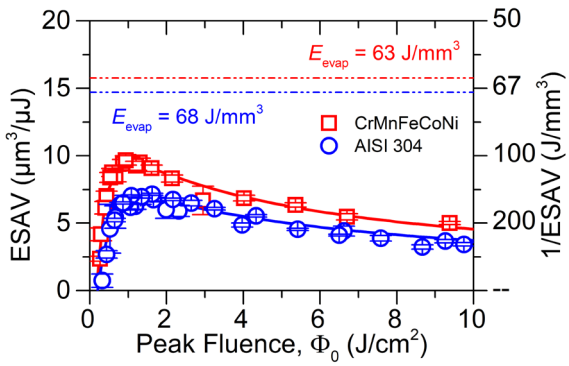

Fig. 2 Reflectance corrected energy specific ablation volume for both investigated alloys (left axis, and right axis inverse value). The total energy density required for evaporation is marked by dashed lines (red CrMnFeCoNi and blue AISI 304).

For energetic considerations, it is common to compare the ablation efficiency with the total energy to vaporize a unit volume [23] although it is known that vaporization in the classical sense does not apply as a driving mechanism in ultrashort pulse laser ablation [24]. For CrMnFeCoNi alloy and AISI 304, this energy is calculated by the rule of mixture to be 63.5 J/mm³ and 67.9 J/mm³ [11], and a comparison with the ablation efficiency shows that for the CrMnFeCoNi alloy only 60% of the applied pulse energy can be assigned to vaporization. For stainless steel, this ratio $\nu = E_{evap}/ESAV^{-1}$ is about 45 %. From the analysis of the effective penetration depths and the ESAV curve it may be concluded that the laser energy deposited in the material follows the Beer-Lambert law. So taking solely the energy absorbed in the ablation volume into account would provide more accurate energy balance. This energy portion is calculated in analogy to [60] as

$$\mathrm{E_{abl}}/\mathrm{E_p} = 1-(\Phi_{\mathrm{thr}}/\Phi_0)[1+\ln(\Phi_0/\Phi_{\mathrm{thr}})]. \tag{3}$$

At the efficiency maximum (in first approximation at $e^2\,F_{thr}$), the fraction of pulse energy absorbed in the ablation volume is roughly 60 %, from which it follows that 40 % of the absorbed energy would remain as residual heat in the material. This approximation is for stainless steel is in good agreement with measurements from literature [25,26]. Including this factor in the preceding consideration of ν shifts the values of

CrMnFeCoNi alloy as well as AISI 304 to about 1 and 0.8, respectively. Therefore, for both alloys the ablation process is energetically in the region of vaporization. No significant effect in the ablation efficiency due to the high configuration entropy of the high entropy alloy CrMnFeCoNi alloy, as is the case with the high-energy particle radiation, could be found. So the driving mechanism, responsible for the increased damage resistance of HEAs to high-energy particle radiation, which is referred to reduced diffusivity of lattice defects, does not significantly affect laser ablation.

4. Summary and Conclusion

Single pulse laser ablation experiments (530 fs, 1056 nm) were performed on polished substrates (RMS roughness < 2 nm) of the CrMnFeCoNi high entropy alloy and AISI 304 stainless steel and the results were compared. The ablation threshold was determined by the D^2 method and is 0.24(1) J/cm² for the CrMnFeCoNi alloy, which is slightly lower than the value for AISI 304 with 0.27(1) J/cm². A comparison of the crater morphology of the two alloys reveals no significant differences. From the ablation depths, it follows that for both alloys the energy deposition in the material may be formulated by the Beer-Lambert law, and the effective penetration depths, determined from the model fit, are in good agreement with the optical penetration depths. The exponential energy density decrease is also revealed in the parabolic shaped crater profiles for fluences around the ablation efficiency maximum. Furthermore, the energy specific ablation volume was calculated. For both alloys, the efficiency maximum is found at approximately 4.5-times the ablation threshold with an absorption corrected ESAV value of 101(8) J/mm³ and 149(11) J/mm³ for the CrMnFeCoNi alloy and AISI 304, respectively. Thus, laser ablation for the CrMnFeCoNi HEA alloy is energetically more efficient than that of the stainless steel alloy. This contrasts with high-energy particle radiation, where high entropy alloys have a lower damage tolerance. Rather, the increase in electron-phonon interaction and reduced thermal conductivity associated with the high chemical complexity of HEAs yields in a confined energy situation during the ablation process. This endows an enhanced ablation efficiency for the CrMnFeCoNi in contrast to AISI 304. In conclusion, we find that the ultrashort pulse laser ablation of the CrMnFeCoNi high entropy alloy is comparable to that of conventional AISI 304 stainless steel, which opens a promising future for precise laser micromachining of high entropy alloys.

Acknowledgements

The authors greatly acknowledge the financial support of this work, which was provided by the Deutsche Forschungsgemeinschaft (DFG) through grants HU 1893/2-1, HU 1893/5-1 and GL 181/56-1.

J.W. gratefully acknowledges the funding of the Erlangen Graduate School in Advanced Optical Technologies (SAOT) by the Bavarian State Ministry for Science and Art.

P.C. and J.M. would like to thank the CEDAMNF Project financed by the Ministry of Education, Youth and Sports of Czech Republic, Project No. CZ.02.1.01/0.0/0.0/15_003/0000358.

References

[1] D.B. Miracle, O.N. Senkov, A critical review of high entropy alloys and related concepts, Acta Mater. 122 (2017) 448–511. https://doi.org/10.1016/j.actamat.2016.08.081.

[2] B. Cantor, I.T.H. Chang, P. Knight, A.J.B. Vincent, Microstructural development in equiatomic multicomponent alloys, Mater. Sci. Eng. A. 375–377 (2004) 213–218. https://doi.org/10.1016/j.msea.2003.10.257.

[3] X. Wang, W. Guo, Y. Fu, High-entropy alloys: emerging materials for advanced functional applications, J. Mater. Chem. A. 9

(2021) 663–701. https://doi.org/10.1039/D0TA09601F.

[4] M. Dada, P. Popoola, S. Adeosun, N. Mathe, High Entropy Alloys for Aerospace Applications, in: Aerodynamics, IntechOpen, 2021: pp. 137–144. https://doi.org/10.5772/intechopen.84982.

[5] E.P. George, D. Raabe, R.O. Ritchie, High-entropy alloys, Nat. Rev. Mater. 4 (2019) 515–534. https://doi.org/10.1038/s41578-019-0121-4.

[6] C. Lu, L. Niu, N. Chen, K. Jin, T. Yang, P. Xiu, Y. Zhang, F. Gao, H. Bei, S. Shi, M.-R. He, I.M. Robertson, W.J. Weber, L. Wang, Enhancing radiation tolerance by controlling defect mobility and migration pathways in multicomponent single-phase alloys, Nat. Commun. 7 (2016) 13564. https://doi.org/10.1038/ncomms13564.

[7] L. Yang, H. Ge, J. Zhang, T. Xiong, Q. Jin, Y. Zhou, X. Shao, B. Zhang, Z. Zhu, S. Zheng, X. Ma, High He-ion irradiation resistance of CrMnFeCoNi high-entropy alloy revealed by comparison study with Ni and 304SS, J. Mater. Sci. Technol. 35 (2019) 300–305. https://doi.org/10.1016/j.jmst.2018.09.050.

[8] C. Momma, B.N. Chichkov, S. Nolte, F. Von Alvensleben, A. Tünnermann, H. Welling, B. Wellegehausen, Short-pulse laser ablation of solid targets, Opt. Commun. 129 (1996) 134–142. https://doi.org/10.1016/0030-4018(96)00250-7.

[9] B. Neuenschwander, B. Jaeggi, M. Schmid, From fs to sub-ns: Dependence of the material removal rate on the pulse duration for metals, Phys. Procedia. 41 (2013) 794–801. https://doi.org/10.1016/j.phpro.2013.03.150.

[10] G. Račiukaitis, M. Brikas, P. Gečys, B. Voisiat, M. Gedvilas, Use of high repetition rate and high power lasers in microfabrication: How to keep the efficiency high?, J. Laser Micro Nanoeng. 4 (2009) 186–191. https://doi.org/10.2961/jlmn.2009.03.0008.

[11] D. Redka, C. Gadelmeier, J. Winter, M. Spellauge, C. Eulenkamp, P. Calta, U. Glatzel, J. Minár, H.P. Huber, Sub-picosecond single-pulse laser ablation of the CrMnFeCoNi high entropy alloy and comparison to stainless steel AISI 304, Appl. Surf. Sci. 544 (2021) 148839. https://doi.org/10.1016/j.apsusc.2020.148839.

[12] C. Gadelmeier, S. Haas, T. Lienig, A. Manzoni, M. Feuerbacher, U. Glatzel, Temperature dependent solid solution strengthening in the high entropy alloy CrMnFeCoNi in single crystalline state, Metals (Basel). 10 (2020) 1–13. https://doi.org/10.3390/met10111412.

[13] J.M. Liu, Simple technique for measurements of pulsed Gaussian-beam spot sizes, Opt. Lett. 7 (1982) 196. https://doi.org/10.1364/ol.7.000196.

[14] M. Garcia-Lechuga, D. Grojo, Simple and robust method for determination of laser fluence thresholds for material modifications: an extension of Liu's approach to imperfect beams, Open Res. Eur. accepted (2021).

[15] O. Armbruster, A. Naghilou, M. Kitzler, W. Kautek, Spot size and pulse number dependence of femtosecond laser ablation thresholds of silicon and stainless steel, Appl. Surf. Sci. 396 (2017) 1736–1740. https://doi.org/10.1016/j.apsusc.2016.11.229.

[16] J. Winter, M. Spellauge, J. Hermann, C. Eulenkamp, H.P. Huber, M. Schmidt, Ultrashort single-pulse laser ablation of stainless steel, aluminium, copper and its dependence on the pulse duration, Opt. Express. 29 (2021) 14561. https://doi.org/10.1364/OE.421097.

[17] N.A. Smirnov, S.I. Kudryashov, P.A. Danilov, A.A. Rudenko, B. Gakovic, D. Milovanović, A.A. Ionin, A.A. Nastulyavichus, S.F. Umanskaya, Microprocessing of a steel surface by single pulses of variable width, Laser Phys. Lett. 16 (2019) 056002. https://doi.org/10.1088/1612-202X/ab0c85.

[18] A. Rudenko, C. Mauclair, F. Garrelie, R. Stoian, J.P. Colombier, Light absorption by surface nanoholes and nanobumps, Appl. Surf. Sci. 470 (2019) 228–233. https://doi.org/10.1016/j.apsusc.2018.11.111.

[19] C. Wu, L. V. Zhigilei, Microscopic mechanisms of laser spallation and ablation of metal targets from large-scale molecular dynamics simulations, Appl. Phys. A Mater. Sci. Process. 114 (2014) 11–32. https://doi.org/10.1007/s00339-013-8086-4.

[20] S. Mu, G.D. Samolyuk, S. Wimmer, M.C. Troparevsky, S.N. Khan, S. Mankovsky, H. Ebert, G.M. Stocks, Uncovering electron scattering mechanisms in NiFeCoCrMn derived concentrated solid solution and high entropy alloys, Npj Comput. Mater. 5 (2019) 1–10. https://doi.org/10.1038/s41524-018-0138-z.

[21] J. Winter, J. Sotrop, S. Borek, H.P. Huber, J. Minár, Temperature-dependent determination of electron heat capacity and electron-phonon coupling factor for Fe0.72Cr0.18Ni0.1, Phys. Rev. B. 93 (2016) 1–8. https://doi.org/10.1103/PhysRevB.93.165119.

[22] J. Furmanski, A.M. Rubenchik, M.D. Shirk, B.C. Stuart, Deterministic processing of alumina with ultrashort laser pulses, J. Appl. Phys. 102 (2007). https://doi.org/10.1063/1.2794376.

[23] J. Lopez, K. Mishchik, G. Mincuzzi, E. Audouard, E. Mottay, R. Kling, Efficient metal processing using high average power ultrafast laser, J. Laser Micro Nanoeng. 12 (2017) 296–303. https://doi.org/10.2961/jlmn.2017.03.0020.

[24] D. Von Der Linde, K. Sokolowski-Tinten, Physical mechanisms of short-pulse laser ablation, Appl. Surf. Sci. 154 (2000) 1–10. https://doi.org/10.1016/S0169-4332(99)00440-7.

[25] B. Bornschlegel, J. Köller, J. Finger, In-situ analysis of heat accumulation during ultrashort pulsed laser ablation, J. Laser Micro Nanoeng. 15 (2020) 56–62. https://doi.org/10.2961/jlmn.2020.01.2010.

[26] J.P. Colombier, P. Combis, E. Audouard, R. Stoian, Guiding heat in laser ablation of metals on ultrafast timescales: An adaptive modeling approach on aluminum, New J. Phys. 14 (2012). https://doi.org/10.1088/1367-2630/14/1/013039.